RESEARCH ARTICLE | NOVEMBER 23 2016

# Low temperature heat capacity of phononic crystal membranes

T. A. Puurtinen; I. J. Maasilta



*AIP Advances* 6, 121902 (2016)
https://doi.org/10.1063/1.4968619

# Low temperature heat capacity of phononic crystal membranes

T. A. Puurtinen[a] and I. J. Maasilta
*Nanoscience Center, Department of Physics, University of Jyvaskyla, P.O. Box 35, FI-40014 Jyväskylä, Finland*

(Received 1 September 2016; accepted 13 November 2016; published online 23 November 2016)

Phononic crystal (PnC) membranes are a promising solution to improve sensitivity of bolometric sensor devices operating at low temperatures. Previous work has concentrated only on tuning thermal conductance, but significant changes to the heat capacity are also expected due to the modification of the phonon modes. Here, we calculate the area-specific heat capacity for thin (37.5 - 300 nm) silicon and silicon nitride PnC membranes with cylindrical hole patterns of varying period, in the temperature range 1 - 350 mK. We compare the results to two- and three-dimensional Debye models, as the 3D Debye model is known to give an accurate estimate for the low-temperature heat capacity of a bulk sample. We found that thin PnC membranes do not obey the 3D Debye $T^3$ law, nor the 2D $T^2$ law, but have a weaker, approximately linear temperature dependence in the low temperature limit. We also found that depending on the design, the PnC patterning can either enhance or reduce the heat capacity compared to an unpatterned membrane of the same thickness. At temperatures below ~ 100 mK, reducing the membrane thickness unintuitively increases the heat capacity for all samples studied. These observations can have significance when designing calorimetric detectors, as heat capacity is a critical parameter for the speed and sensitivity of a device.  [http://dx.doi.org/10.1063/1.4968619]



## I. INTRODUCTION

The two observables that typically define the thermal properties of a material are thermal conductivity and heat capacity. Out of those, thermal conductivity attracts more attention, as there are many applications where one would like to change it, such as improving thermoelectrics[1] or low-temperature radiation detectors.[2] In many cases, it is specifically the phononic thermal properties that are under interest, and large modifications to thermal conductivity are possible even at room temperature by changing the scattering probability of phonons by impurities, nanoparticles, surface roughness etc.[3] On the other hand, heat capacity is typically considered to be a material parameter, determined simply by the bulk phonon density of states.[4]

In addition to disordered scatterers, recent years has also seen the introduction of periodic structures, or phononic crystals (PnC)[5] for thermal transport control. For PnC's there is the question, whether the periodicity is still just an incoherent array of scatterers, or whether wave coherence can play a role and modify the phonon dispersion relations.[6] Most of the experimental studies so far have concentrated on thermal conductivity at intermediate-to-room temperatures, and studied either on 2D holey structures[7–10] or 1D superlattices.[11,12] At those temperatures, diffusive scattering is definitely still operational,[13,14] meaning that the effect of coherence is only partial, if existing at all.

However, at sub-Kelvin temperatures, where most of the ultrasensitive radiation detectors operate, diffusive scattering mechanisms die out and the effect of periodicity is solely through the coherent

[a]Electronic mail: tuomas.a.puurtinen@jyu.fi

 

mechanism. In that case the phonon band structure of the solid material is strongly modified and can even form frequency bands where propagating phonons do not exist.[15,16] The influence of coherent scattering on reducing thermal conductance was recently demonstrated in micron scale 2D PnC hole structures at ultra-low temperatures below 1K,[16] and calculations also exist for smaller periodicities,[17–19] where an enhancement is also predicted.[18,19] Numerical work also exists on the coherence effects in 1D beam geometry.[20,21]

Here, we calculate, in contrast, the coherent effect of a periodic 2D PnC hole structure on the heat capacity $C$ of a thin membrane. It is already known[22,23] that by merely suspending a thin membrane of thickness below $\sim 1\mu$m, the low-temperature heat capacity is strongly modified from the 3D Debye law, due to the formation of the Lamb modes. In this paper, we investigate, how the PnC structure modifies this further. This has also practical relevance, because heat capacity is an important variable in bolometric detectors, as their noise properties depend sensitively on the heat capacities of different parts of the device.[24,25] Moreover, in the calorimetric (energy resolving) mode, the energy resolution is strongly dependent on the heat capacity.[26] In this work we calculate the heat capacities for two common membrane materials used in low temperature devices, silicon and silicon nitride, and compare how PnC patterns of different periodicity and membrane thickness affect the heat capacity. It is seen that by adjusting the lattice constant and the thickness, the heat capacity of the membrane can be tuned roughly by an order of magnitude, and both a reduction and an enhancement of $C$ can be observed. The results are also compared to the Debye 3D and 2D models, which give roughly a correct estimate for $C$ at $\sim 300$ mK, but predict orders of magnitude too small $C$ at lower temperatures due to the much weaker temperature dependence $C \sim T$ in the PnCs. The differences between the heat capacities of Si and SiN are minor.

## II. HEAT CAPACITY

Low temperature phononic heat capacity $C = C(T)$ at temperature $T$ of an insulator is given by

$$C(T) = \frac{\partial U(T)}{\partial T} = \frac{\partial}{\partial T} \sum_{\boldsymbol{k},j} \frac{\hbar\omega_j(\boldsymbol{k})}{\exp(\hbar\omega_j/k_\mathrm{B}T) - 1}, \tag{1}$$

where $U$ is the internal energy of the crystal, and where the summation goes over all phonon modes $j$ with dispersion relations $\omega_j = \omega_j(\boldsymbol{k})$ and wave vectors $\boldsymbol{k}$. As usual, $\hbar$ is the Planck constant and $k_\mathrm{B}$ is the Boltzmann constant. By changing the summation to integration over the $K$-space, carrying out the temperature differentiation and dividing by the area we get an area-specific heat capacity as

$$C_\mathrm{A}(T) = \frac{\hbar^2}{16\pi^2 k_\mathrm{B} T^2} \sum_j \int_K \mathrm{d}\boldsymbol{k} \frac{\omega_j^2(\boldsymbol{k})}{\sinh^2(\hbar\omega_j/2k_\mathrm{B}T)} \tag{2}$$

that has the units $\mathrm{J/K \cdot m^2}$.

In the 2D Debye approximation, integration over the phonon branches is only carried over the two transversal and one longitudinal bulk phonon modes with velocities $c_\mathrm{t}$ and $c_\mathrm{l}$. Assuming isotropy, the $K$ integral becomes one dimensional, and by the change of variable $x = \hbar c_j k/2k_\mathrm{B}T$ we end up with

$$C_\mathrm{2D} = \frac{3\zeta(3)}{\pi} \frac{k_\mathrm{B}^3}{\hbar^2} \left( \frac{2}{c_\mathrm{t}^2} + \frac{1}{c_\mathrm{l}^2} \right) T^2 \tag{3}$$

where $\zeta$ is the Riemann zeta function. We immediately notice that area-specific $C_\mathrm{2D}$ does not depend on the membrane thickness. The 2D Debye model differs from the 3D Debye model (also known by the Debye $T^3$ law)

$$C_\mathrm{3D} = \frac{4\pi^3}{15} \frac{k_\mathrm{B}^4}{\hbar^3} \left( \frac{2}{c_\mathrm{t}^3} + \frac{1}{c_\mathrm{l}^3} \right) T^3 \tag{4}$$

of the volume-specific heat capacity by a lower order temperature dependence (different power law) and the coefficient. The Debye $T^3$ model is known to fit well to the experimental heat capacity measurements for most insulating materials from the low temperature limit to room temperature.[27]

Using the above formulas, we calculated the heat capacity for various Si and SiN phononic crystal membranes with a comparison to full unpatterned membranes of the same materials. Elastic material parameters used for SiN were $E$ = 250 GPa, $\nu = 0.23$, $\rho = 3100$ kg/m$^3$. Shear constant $G = E/(2(1 + \nu)) \approx 101.6$ GPa can be calculated from the given parameters. For Si in the (100) orientation (cubic symmetry) we used $E_i$ = 130 GPa, $\nu_{ij} = 0.28$, $G_{ij}$ = 79.6 GPa, $i,j = x, y, z$ $i \neq j$, and $\rho = 2330$ kg/s.[28] The PnC membranes had cylindrical holes in a square lattice configuration perpendicular to the membrane surfaces (in x,y plane), the same geometry as in Ref. 19. In the case of Si, the hole pattern was aligned with the underlying atomic Si crystal lattice, in order to enhance the Si anisotropy effects. SiN was considered to be isotropic, so no alignment effects exist. Using a fixed hole filling fraction $f = 0.7$, we changed the lattice constants over the range 250 nm, 500 nm, 1 $\mu$m and 2 $\mu$m, alongside with the membrane thicknesses over the range 37.5 nm, 75 nm, 150 nm and 300 nm.

The average phonon number at each temperature is given by the Bose-Einstein distribution $n(\omega, T) = (\exp(\hbar\omega/k_B T) - 1)^{-1}$, which has an exponentially vanishing tail as $\omega \to \infty$. A temperature dependent upper limit for the frequency $\nu = \omega/(2\pi)$ can thus be found so that the modes sufficiently describe the thermal properties of the material. For instance, at 1 mK, $n(\omega, T) = 1$ for $\nu \approx 0.014$ GHz, above which the occupation starts to die off exponentially. At $T$ = 100 mK, $n(\omega, T) = 1$ for $\nu \approx 1.4$GHz, and at $T$ = 350 mK, $\nu \approx 5$ GHz. To have enough accuracy, phonon dispersion relations have to be calculated to about order of magnitude higher frequencies, in this study therefore up to $\nu \approx 50$ GHz. However, it is often best to compare numerically how the number of modes affects the results so that a sufficient number of modes can be chosen.

First, using the finite element method we numerically calculated the phonon modes (displacement fields) and respective eigenfrequencies in the linear elasticity theory. The Bloch boundary condition was used on the boundaries of the PnC periodicity cell.[16] The dispersion relations $\omega_j$ were calculated over the full 2D irreducible Brillouin zone on $\sim 700 - 4200$ wave vectors. Frequency branches were calculated up to (at least) $\nu = 50$ GHz resulting to $\sim 500 - 5000$ eigenfrequencies for each wave vector. This was found to give sufficient results up to 350 mK temperature. Finite element method was also used for the (orthotropic) unperforated Si membrane dispersion relations using an artificial periodicity cell, a cubic block of material, together with the Bloch boundary conditions as the model domain. For unperforated SiN membranes, the dispersion relations were analytically calculated using Rayleigh-Lamb theory.[29]

A general understanding of the relative order and the group velocities of the phonon modes can be obtained by visually comparing the phonon frequency spectra in Fig. 1 where they are shown for membranes with thickness $h$ = 300 nm (left and center) and a lattice constant of the unit cell $a$ = 500 nm. The rightmost graph shows the spectrum for a PnC membrane with $h$ = 37.5 nm. The choice of lattice constant is artificial for the full membrane samples and is used here to help

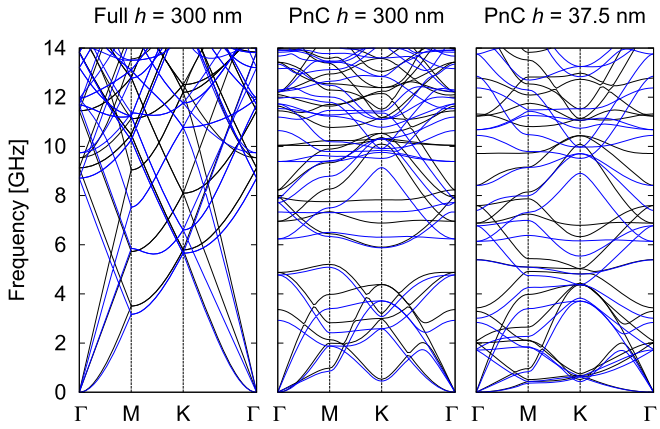


FIG. 1. Dispersion relations for Si (blue) and SiN (black) PnCs with two thicknesses (center and right) and full, unperforated membranes (left) along the irreducible Brillouin zone edges (artificial for the full membranes). Spacing of the symmetry points reflects their relative distances in the $K$-space. All plots share the same lattice constant $a$ = 500 nm.

with the comparison of the curves. We notice that the spectrum of the Si full membrane is slightly shifted to lower frequencies vs. the SiN membrane. This observation can be explained by considering the material parameters. There is a significant difference in hardness of these two materials, which increases phonon frequencies for SiN, but the lower density of Si reduces this effect. Overall, the spectra look surprisingly similar, although Si anisotropy is clearly visible, especially for the lowest shear mode (the second lowest branch) in the Γ-K direction. In the case of 300 nm PnC membranes, hole patterning clearly modifies the spectral features in comparison to full membranes. Frequency bands appear to be generally flatter resulting to low group velocities but at the same time higher densities of states. There is also a spectral gap at ~ 5.5 GHz for the 300 nm PnC membrane.

Interestingly, comparing the spectra of the PnC membranes with different thicknesses (center and right) a lot of similarities can be found. Especially, in the low frequency limit the modes with linear $k$-dependence do not depend on the thickness. However, the first antisymmetric flexural mode clearly depends on the thickness, and it seems to have roughly a quadratic $k$-dependence similarly to its full membrane counterpart (see e.g. Kühn *et al.*[22]).

In Fig. 2 we show the area-specific heat capacities of the non-PnC and PnC membranes in a temperature range from 1 mK to 350 mK. Overall, Si and SiN heat capacities have very similar features with roughly a constant factor difference between them over the whole temperature range investigated. This is not surprising, considering that there are no significant differences in the dispersion relations. Si has the higher heat capacity compared to SiN, which is caused by the fact that dispersion relations are generally shifted to a lower frequency range. This observation agrees with calculations of low temperature thermal conductance in thin membranes, for which it is well understood that lower speed of sound results in higher thermal conductance.[30] This completely differs from the more intuitive behavior observed at room temperatures where thermal conductivity always grows with a higher speed of sound.[4]

Interestingly, for all periods and thicknesses, there is a clear transition region around 100 mK to 200 mK, where the effect of the thickness with respect to the heat capacity changes sign. At

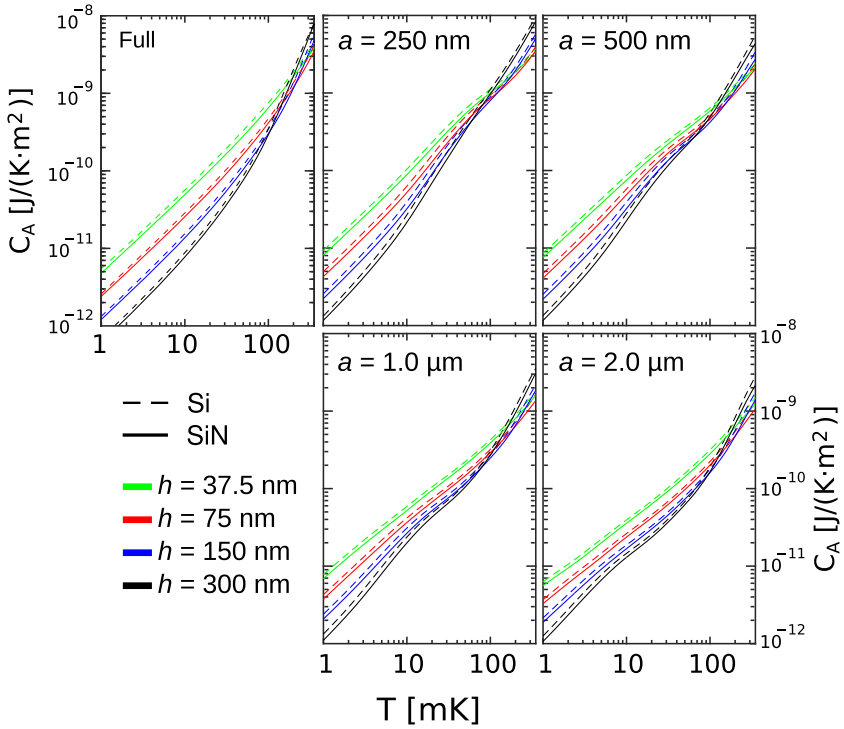


FIG. 2. Area-specific heat capacity of Si (dashed curves) and SiN (solid curves) hole patterned PnC membranes with various thicknesses $h$ and PnC lattice constants $a$ (values shown within the plots). Hole filling factor $f = 0.7$.

temperatures below the transition, heat capacity *increases* for thinner membranes, but at temperatures above the transition region, it is reduced. This effect is caused by the first (lowest) anti-symmetric (flexural) Lamb mode $A_0$ that has quadratic $k$-dependence at the $k \to 0$ limit. Looking at the integrand in Eq. 2 we see that it is suppressed by the denominator as $\omega$ increases. Therefore, modes residing in the low frequency range have a larger contribution to the total heat capacity. Specifically, the $A_0$ mode is scaled to lower frequencies as the thickness is reduced, causing heat capacity to increase accordingly. For instance, at 1 mK the $A_0$ mode accounts for 93% of the total heat capacity for the 300 nm SiN PnC membrane with 250 nm periodicity, and 99% for the similar, but thinner 37.5 nm membrane. At higher temperatures, more modes come into play and the contribution of the $A_0$ mode becomes less distinct.

Another interesting feature of the curves is that near the transition region at 100 mK (a typical operating temperature for low-$T$ sensors), the sensor designer has relatively limited control of the heat capacity with the thickness of the membrane. Instead, the results suggest that the PnC lattice constant is the more effective design parameter for tuning heat capacity at 100 mK temperature and above.

In Fig. 3 we compare the temperature dependence of the heat capacity to the 2D and 3D Debye models, Eqs. (3–4). Here we used a PnC material filling fraction $f_{\mathrm{mat}} = 0.3$ as a common multiplier to the Debye models so that they take into account the area density of the membranes. The wave velocities used for the SiN transversal and longitudinal modes were $c_{\mathrm{t}} = 5726$ m/s and $c_{\mathrm{l}} = 9669$ m/s, respectively. The Debye models clearly do not capture the low temperature limit behavior correctly. The phononic crystal heat capacity curves generally have a much weaker $C \sim T$ dependence (at the low $T$ limit), which means that an error of many orders of magnitude could be made if Debye models are used for estimation below $T < 100$ mK. In addition, the 3D Debye model does not capture the folding effect with the membrane thickness, where the dependence on thickness changes sign. However, at higher temperatures above the transition region (within the limits of this study), both 2D and 3D models can give a rough estimate, but accurate only at the order of magnitude level.

Similarly to the emitted power enhancement comparison in Ref. 19 we compare in Fig. 4 how the SiN PnC patterning can enhance or reduce the heat capacity compared to the similar full SiN membrane. At the 100 mK temperature point, we see that for all the considered thicknesses both enhancement and reduction can be obtained by choosing an appropriate PnC patterning period. The enhancement factor is higher for smaller lattice constants, and lower for larger constants. The highest enhancement of 427% is reached for the 300 nm PnC membrane with 250 nm lattice constant at a temperature of 50 mK. We also notice that the maximum heat capacity enhancement is higher than the maximum emitted power (thermal conductance) enhancement ($\sim 210\%$, $T = 30$ mK).[19] The largest reduction of $\sim 80\%$ occurs at 350 mK (high $T$ limit of this study), although, the trend of the curves indicates that a greater reduction percentage will take place at even higher temperatures. Let

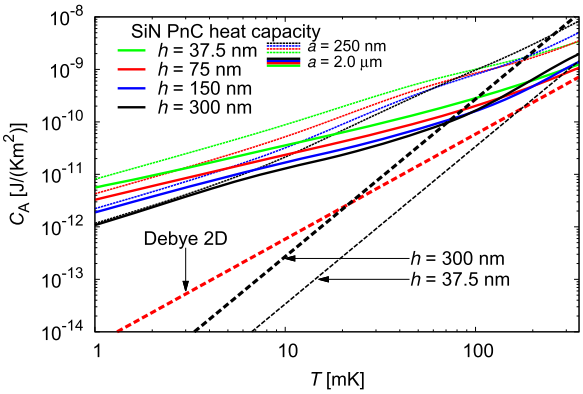


FIG. 3. 2D and 3D Debye models compared with the calculated PnC heat capacities. Solid ($a = 2.0$ $\mu$m) and thin dashed ($a = 250$ nm) curves illustrate the exact theory for SiN membranes with different thicknesses represented by the color. Red dashed curve is the 2D Debye model, thick black dashed curve is the 3D Debye model for the 300 nm membrane, and thin black dashed curve is the 3D model for a 37.5 nm membrane.

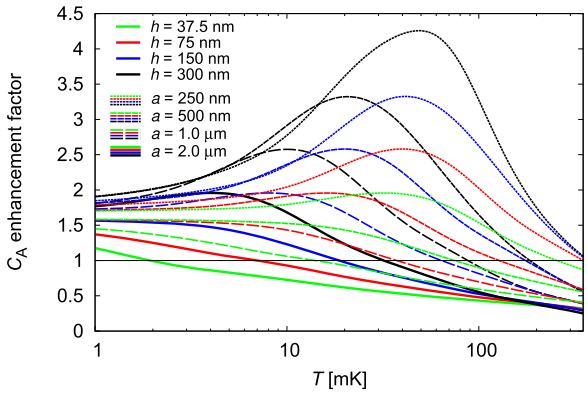


FIG. 4. Area-specific heat capacity enhancement factor for SiN PnC membranes with different thicknesses and lattice constants. Thin black line shows the full membrane heat capacity level, scaled to be equal for each different thickness.

us reiterate how strange this heat capacity enhancement really is: By removing matter, heat capacity can increase!

## III. CONCLUSIONS

We calculated the area-specific heat capacity of silicon and silicon nitride 2D phononic crystal membranes with periodic, square lattice hole patterns, and compared the results to those of Debye models and full, unperforated membranes of the same materials. We found that in the 50 - 200 mK temperature range, PnC patterning can be used to either enhance or reduce the heat capacity of the membrane. The strength and sign of the effect depends on the lattice constant of the pattern. We found that the Si and SiN heat capacities do not have major distinctive differences, although their material properties do differ noticeably.

Common to both materials at a fixed temperature, by varying the membrane thickness and the PnC period (over the values chosen in this work), one can tune the heat capacity within an interval of an order of magnitude. We showed that at the low temperature limit, the heat capacity follows $T^1$ power law similar to unperforated membranes,[22] and because of that, the Debye $T^2$ and $T^3$ models do not yield good estimates in general. Close to the temperature $\sim 100$ mK, for all investigated membranes, there is a transition region where the heat capacity power law changes. This occurs at slightly different temperatures for membranes with different thicknesses, causing a change to the order of the curves. Below this transition point, thinner membranes have a higher heat capacity, which is completely opposite to the behavior at higher temperatures above the transition, where the typical bulk behavior (thicker film, higher heat capacity) is approached. For temperatures above the transition point, the Debye $T^3$ model thus captures the direction of the thickness dependence correctly, but can only be used to give a good estimate up to an order of magnitude of at the temperature range studied here.

## ACKNOWLEDGMENTS

This work was supported by the Academy of Finland project No. 260880. We acknowledge the use of CSC-IT Center for Science supercomputing facilities.

[1] A. J. Minnich, M. S. Dresselhaus, Z. F. Ren, and G. Chen, Energ. Environ. Sci. **2**, 466 (2009).
[2] I. J. Maasilta, T. A. Puurtinen, Y. Tian, and Z. Geng, J. Low Temp. Phys. **184**, 211 (2016).
[3] D. G. Cahill, P. V. Braun, G. Chen, D. R. Clarke, S. Fan, K. E. Goodson, P. Keblinski, W. P. King, G. D. Mahan, A. Majumdar, H. J. Maris, S. R. Phillpot, E. Pop, and L. Shi, Applied Physics Reviews **1**, 011305 (2014).
[4] J. P. Wolfe, *Imaging Phonons: Acoustic Wave Propagation in Solids* (Cambridge University Press, Cambridge, 1998).
[5] A. Khelif and A. Adibi, Eds., *Phononic Crystals, Fundamentals and Applications* (Springer, 2016).
[6] M. Maldovan, Nature Materials **14**, 667 (2015).
[7] J. Tang, H.-T. Wang, D. H. Lee, M. Fardy, Z. Huo, T. P. Russell, and P. Yang, Nano Lett. **10**, 4279 (2010).
[8] S. Alaie, D. F. Goettler, M. Su, Z. C. Leseman, C. M. Reinke, and I. El-Kady, Nat. Commun. **6**, 7228 (2015).
[9] R. Anufriev, J. Maire, and M. Nomura, Phys. Rev. B **93**, 045411 (2016).

[10] J.-K. Yu, S. Mitrovic, D. Tham, J. Vargese, and J. R. Heath, Nat. Nanotech. **5**, 718 (2010).
[11] M. N. Luckyanova, J. Garg, K. Esfarjani, A. Jandl, M. T. Bulsara, A. J. Schmidt, A. J. Minnich, S. Chen, M. S. Dresselhaus, Z. Ren, E. A. Fitzgerald, and G. Chen, Science **338**, 936 (2012).
[12] J. Ravichandran, A. K. Yadav, R. Cheaito, P. B. Rossen, A. Soukiassian, S. J. Suresha, J. C. Duda, B. M. Foley, C.-H. Lee, Y. Zhu, A. W. Lichtenberger, J. E. Moore, D. A. Muller, D. G. Schlom, P. E. Hopkins, A. Majumdar, R. Ramesh, and M. A. Zurbuchen, Nature Materials **13**, 168 (2014).
[13] A. Jain, Y.-J. Yu, and A. J. H. McGaughey, Phys. Rev. B **87**, 195301 (2013).
[14] N. Ravichandran and A. J. Minnich, Phys. Rev. B **89**, 205432 (2014).
[15] Y. Pennec, J. O. Vasseur, B. Djafari-Rouhani, L. Dobrzynski, and P. A. Deymier, Surf. Sci. Rep. **65**, 229 (2010).
[16] N. Zen, T. A. Puurtinen, T. J. Isotalo, S. Chaudhuri, and I. J. Maasilta, Nat. Commun. **5**, 3435 (2014).
[17] R. Anufriev and M. Nomura, Phys. Rev. B **93**, 045410 (2016).
[18] R. Anufriev and M. Nomura, Phys. Rev. B **91**, 245417 (2015).
[19] T. A. Puurtinen and I. J. Maasilta, Crystals **6**(6), 72 (2016).
[20] A. N. Cleland, D. R. Schmidt, and C. S. Yang, Phys. Rev. B **64**, 172301 (2001).
[21] T. Puurtinen, P. Neittaanmäki, and L. Baskin, Physica E Low Dimens Syst Nanostruct. **44**(7–8), 1189 (2012).
[22] T. Kühn, D. V. Anghel, J. P. Pekola, M. Manninen, and Y. M. Galperin, Phys. Rev. B **70**, 125425 (2004).
[23] O. V. Fefelov, J. Bergli, and Y. M. Galperin, Phys. Rev. B **75**, 172101 (2007).
[24] I. J. Maasilta, AIP Advances **2**, 042110 (2012).
[25] K. M. Kinnunen, M. R. J. Palosaari, and I. J. Maasilta, J. Appl. Phys. **112**, 034515 (2012).
[26] Ch. Enss, Ed., *Cryogenic Particle Detection* (Springer, 2005).
[27] N. W. Ashcroft and N. David Mermin, *Solid State Physics* (Saunders, 1976).
[28] M. A. Hopcroft, W. D. Nix, and T. W. Kenny, J. Microelectromech. Syst. **19**, 2 (2010).
[29] K. F. Graff, *Wave Motion in Elastic Solids* (Dover, New York, 1991).
[30] T. Kühn and I. J. Maasilta, J. Physics: Conf. Ser. **92**, 012082 (2007).